https://doi.org/10.1016/j.epsr.2022.108564

The Impact of DFIG Control Schemes on The Negative-Sequence based Differential Protection

Yuanzhu Chang, Mingxuan Zhao
Department of Electrical Engineering
Polytechnique Montréal
Montreal, Canada
yuanzhu.chang@polymtl.ca, mingxuan.zhao@polymtl.ca

Ilhan Kocar
Department of Electrical Engineering
The Hong Kong Polytechnic University
Hong Kong SAR
ilhan.kocar@polyu.edu.hk

***Abstract*—Negative-sequence currents at the transmission line terminals are widely adopted in differential protection to achieve excellent sensitivity. The underlying principle is that the traditional power sources (synchronous generators) can be treated as inductive reactance in the negative-sequence network. However, for the transmission lines connected to Doubly-Fed Induction Generator (DFIG) based wind parks (WPs), the negative-sequence currents are controlled by fault-ride-through (FRT) solutions. This paper first analyzes the phasor characteristics between negative-sequence voltage and current of a DFIG-based WP under three typical FRT solutions, and then evaluates their impact on the dynamic performance of negative-sequence differential protection elements (87LQ). The analysis indicates that a certain FRT control strategy would make DFIG-based WP provide capacitive current into the negative-sequence network. This impacts the sensitivity and even results in maloperation as shown for the first time in this work. The analytical results are validated with detailed time domain models and simulations in Simulink.**

***Index Terms*--Doubly Fed Induction Generator (DFIG), differential protection, negative sequence, short circuit, unsymmetrical fault.**

I. INTRODUCTION

Line current differential (LCD) protection element (denoted by 87L in [1]) is considered as one of the most secure and dependable schemes in use today [2]. By comparing the current phasors at the local and remote terminals, 87L provides excellent sensitivity in discriminating internal and external faults [3]. In the digital implementations of modern current differential protection, negative-sequence currents (other than zero-sequence or phase currents) are preferred to detect unsymmetrical faults because of its superior invulnerability to line-charging currents, current transformer (CT) saturation and large fault resistance [4]-[8]. However, the negative-sequence differential protection element (referred to as 87LQ in [6] or 87_{2L} in [3]) operates on the assumption that every power source can be treated as constant inductive reactance in the negative-sequence network. As a result, since the source of the negative-sequence voltage is located at the fault point, negative-sequence current phasors of a given two terminals are 180° out of phase under external fault condition and in phase under internal fault condition. Unlike synchronous generators (SGs) in traditional power systems, wind parks (WPs) and other inverter-based resources (IBRs) would enable various fault-ride-through (FRT) strategies and solutions to comply with different grid code requirements [9]. Consequently, from the perspective of power system, negative-sequence currents contributed by IBRs are determined by controllers and it could be capacitive rather than inductive [10]. This change in the phase relationship introduces an emerging challenge for protection engineers, namely what and how much impact there will be as the integration of IBRs such as WPs [11] is on the rise.

The existing 87L operates either on the percentage or alpha-plane (current ratio) differential principles. Its digital implementations have been well explained in [1]-[8]. In the early studies, IBRs have been simply regarded as weak-infeed sources and thus 87L has been considered to be immune and not susceptible to maloperation due to IBRs [5], [12]. However, recent research shows otherwise. In [13], poor performance of 87L is analyzed for distribution networks and T-connected inverter-interfaced distributed generators (IIDGs). Reference [14] reveals that the unbalanced charging current introduced by long high voltage submarine cables would affect the sensitivity of 87L in offshore WP scenarios. References [15] and [16] show that 87LQ operating on alpha-plane differential principle would even mis operate when full-size converter (FSC) based wind turbine generators (WTGs) (also referred to as Type-IV WTGs) are controlled by the traditional coupled sequence control (CSC).

To the best of authors' knowledge, although the impact of WTGs on various protection elements have been studied [17]-[21], the phasor characteristics of negative-sequence current contributed by Doubly-Fed Induction Generator (DFIG) based WTGs (also referred to as Type-III WTGs) as well as its impact on 87LQ have not been evaluated and analyzed in detail, especially by considering various FRT solutions. To fill this gap, two main contributions are made in this paper. It is discovered that, when the negative-sequence control of DFIG-based WTG is employed to eliminate the double grid frequency oscillations in electromagnetic torque (described as positive negative sequence control on electromagnetic torque

Submitted to the 22nd Power Systems Computation Conference (PSCC 2022).

and denoted by PNSC-Tem), 87LQ may misinterpret internal short circuits as external faults and therefore does not operate. The negative-sequence capacitive currents contributed by DFIG-based WTGs are identified as the reason of this kind of maloperation.

The rest of the paper is organized as follows. The operating principles and settings of 87LQ are briefly introduced in Section II. Phasor characteristics between negative-sequence voltage and current of a DFIG-based WTG are analyzed under three different FRT solutions in Section III. The dynamic performance of 87LQ is evaluated under crowbar protection and other FRT control strategies in Section IV. Section V evaluates the impact of fault locations and short circuit strengths on the maloperation. Finally, conclusions are given in Section V.

II. Protection Principles and Settings

The basic operating principles and typical settings of 87LQ are briefly introduced in this section. It is highlighted that the inherent sensitivity of 87LQ is built on the negative-sequence inductive currents provided by power sources.

A. Traditional Power System and Fault Analysis

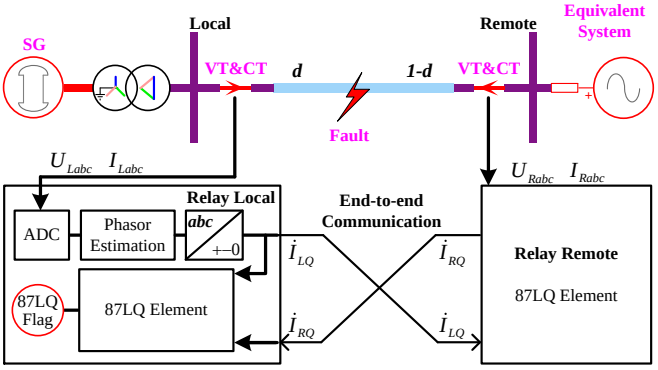

Figure 1. 2-bus traditional power system under 87LQ protection.

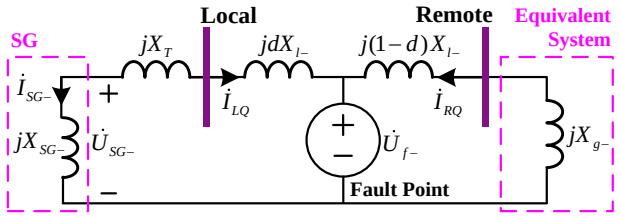

Figure 2. Negative-sequence network of the traditional power system.

A transmission line protected by 87LQ in a traditional power system is shown in Fig. 1. The negative-sequence network of this traditional power system is shown Fig. 2. In the negative-sequence network, resistances are ignored, and both the SG and the equivalent system are represented by inductive reactances X_{SG-} and X_{g-}, respectively. Per nodal analysis, the negative-sequence current phasors at the local and remote buses ($\dot{I}_{LQ}$ and $\dot{I}_{RQ}$) have the same magnitudes but opposite phase angles under normal or external unsymmetrical fault conditions. However, following the inception of an internal unsymmetrical fault on the protected line, $\dot{I}_{LQ}$ and $\dot{I}_{RQ}$ would become in phase and are given as follows

$$\dot{I}_{LQ}=\frac{-\dot{U}_{f-}}{j(X_{SG-}+X_T+dX_{l-})} \quad \dot{I}_{RQ}=\frac{-\dot{U}_f}{j[(1-d)X_{l-}+X_{g-}]} \tag{1}$$

where d is the fault location in per unit. Given that, $\dot{I}_{LQ}$ and $\dot{I}_{RQ}$ are ideally in phase during an internal fault, the angle difference between them is employed in 87LQ to achieve high sensitivity in discriminating internal and external unsymmetrical faults. It's worth noting that this kind of phase relationship is based on the negative-sequence inductive current provided by the SG: the negative-sequence current phasor $\dot{I}_{SG-}$ lags negative-sequence voltage phasor $\dot{U}_{SG-}$ by 90°.

If a new power source provides capacitive current into the negative-sequence network behaving like a capacitive reactance ($-X_{C-}$) as shown in Fig. 3, $\dot{I}_{LQ}$ and $\dot{I}_{RQ}$ would become

$$\dot{I}_{LQ}=\frac{-\dot{U}_{f-}}{j(-X_{C-}+X_T+dX_{l-})} \quad \dot{I}_{RQ}=\frac{-\dot{U}_f}{j[(1-d)X_{l-}+X_{g-}]} \tag{2}$$

If $X_{C-}>X_T+dX_{l-}$, their angle difference will still be 180° even under the same internal unsymmetrical fault. This scenario does not exist in the traditional power system but become possible when IBRs are integrated into the grid.

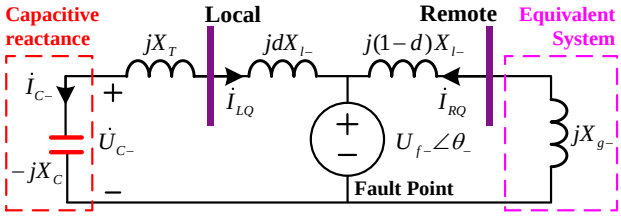

Figure 3. Negative-sequence network when the power source provides capacitive current.

B. 87LQ Operating on Percentage Differential Principle

Traditional 87LQ protection schemes first convert $\dot{I}_{LQ}$ and $\dot{I}_{RQ}$ into operating current (I_{OP}) and restraining current (I_{RT}) by

$$I_{OP}=\left|\dot{I}_{LQ}+\dot{I}_{RQ}\right| \quad I_{RT}=\left|\dot{I}_{LQ}\right|+\left|\dot{I}_{RQ}\right| \tag{3}$$

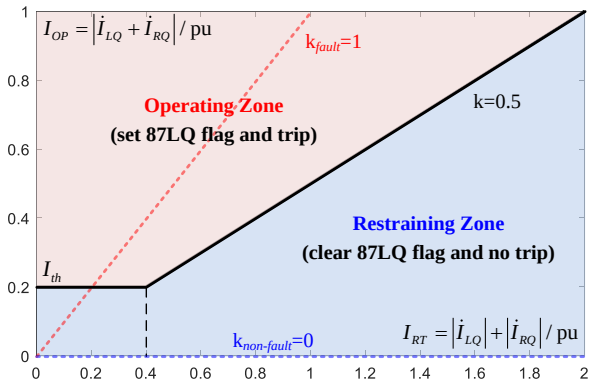

Figure 4. Dual-slope percentage differential principle of 87LQ.

Then, the trip decision is made by comparing I_{OP} and I_{RT} according to the percentage principle shown in Fig. 4. For an internal unsymmetrical fault in the traditional power system, since $\dot{I}_{LQ}$ and $\dot{I}_{RQ}$ are in-phase, I_{OP}=I_{RT} and the trajectory is located on the line with a slope of unity (shown as the red dashed line in Fig. 4). Otherwise, the trajectory is located at the origin for normal operating conditions and on the positive real axis (shown as the blue dashed line in Fig. 4) for external unsymmetrical faults. A trip signal will be issued when I_{OP} is above the pickup threshold I_{th} and is larger than I_{RT} by a factor of k. Typical 87LQ settings are 0.2 pu for I_{th} and 0.5 for k.

C. 87LQ Operating on Alpha-plane Differential Principle

Apart from the percentage differential principle, alpha-plane differential principle has been proposed and used in 87L schemes to achieve better immunity to CT saturation and channel asymmetry [22]. The alpha-plane principle calculates the complex current ratio $\dot{I}_{RQ}/\dot{I}_{LQ}$ using both the amplitude and phase angle. The calculated current ratio is plotted on a complex plane called alpha plane. For an internal unsymmetrical fault in a traditional power system, the current ratio is located on the positive real axis (shown as the red solid line in Fig. 5) since $\dot{I}_{LQ}$ and $\dot{I}_{RQ}$ are in-phase. Under normal operating condition and external unsymmetrical fault condition, this current ratio becomes -1. The trip decision is made if the current ratio falls outside of the restraining zone, defined by parameters R and α as shown in Fig. 5. Typical 87LQ settings are R=5 and α=240°.

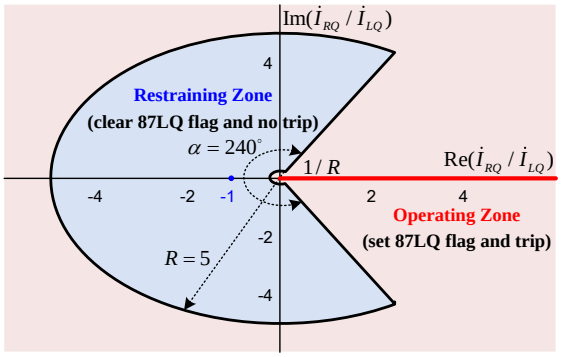

Figure 5. Alpha-plane differental principle of 87LQ.

III. Phasor Characteristics between Negative-sequence Voltage and Current of a DFIG-based WP

This section analyzes the phasor relationship between the negative-sequence voltage and current of a DFIG-based WP under three different FRT solutions. The objective is to evaluate how inductive the current is.

A. Negative-sequence Phasor Characteristics of a DFIG-based WTG under Crowbar Protection

The schematic of a DFIG-based WTG is shown in Fig. 6. The rotor and grid side converters (RSC and GSC) are rated according to the slip power which is typically 30% of the rated power of the WTG. Under a severe voltage unbalance, the rotor current may exceed the capacity of the RSC, especially when using the traditional CSC [23]. To protect the converters from overcurrent, crowbar circuit is widely used to bypass the rotor winding.

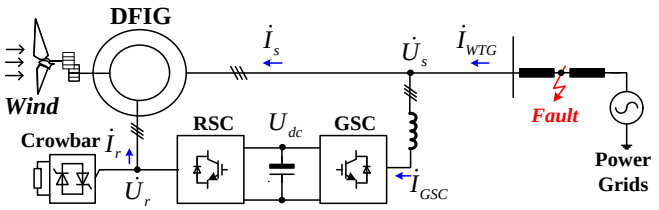

Figure 6. Schematic of a DFIG-based WTG.

The negative-sequence current of the DFIG under crowbar protection has been analyzed in [24]. The negative-sequence current is mainly contributed by the stator winding and expressed by

$$\dot{I}_{WTG-} \approx \dot{I}_{s-} = \dot{U}_{s-} / Z_{DFIG-} \tag{4}$$

where Z_{DFIG-} stands for the negative-sequence equivalent impedance of the DFIG during the crowbar protection.

$$Z_{DFIG-} = R_s + j\omega_1 L_s \frac{j(2-s)\omega_1 \sigma L_r + (R_r + R_{cb})}{j(2-s)\omega_1 L_r + (R_r + R_{cb})} \tag{5}$$

TABLE I. Parameters of a 1.5MW DFIG-base WTG

Parameter	Value	Parameter	Value
Voltage base for p.u.	469.486 V	U_{dc}	1150 V
Rated active power	1.5 MW	P^*	0.9 pu
Power base for p.u.	1.667 MVA	Q^*	0 pu
R_s	0.023 pu	σ	0.108
R_r	0.016 pu	$\omega_1 L_s$	3.08 pu
R_{cb}	0.140 pu (0.25Ω)	$\omega_1 L_r$	3.06 pu
ω_1	120π rad/s	$\omega_1 L_m$	2.9 pu
s	-0.2	I_{RSC_max}	1.2 pu
K_{V+}	2	K_{V-}	2

Inserting the practical parameters for a 1.5 MW DFIG-based WTG shown in Table I into (5), Z_{DFIG-} as well as the negative-sequence current phasor are calculated as

$$Z_{DFIG-} = 0.087+j0.333 \quad \dot{I}_{s-} = \dot{U}_{s-} / (0.344\angle 75.4^\circ) \tag{6}$$

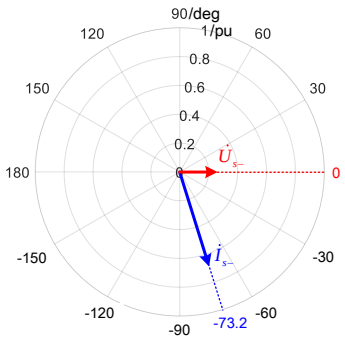

Figure 7. The phasor diagram of the negative-sequence voltage and current of a DFIG under crowbar protection.

The phasor relationship between the negative-sequence voltage and current is shown in Fig. 7. It shows that, when the

crowbar circuit is triggered, the DFIG-based WTG behaves as an inductance in series with a resistance in the negative-sequence system.

B. Negative-sequence Phasor Characteristics of DFIG-based WTG under PNSC-Tem

Under a mild voltage unbalance, the PNSC-Tem can be employed to eliminate the double grid frequency oscillations in electromagnetic torque [25], [26]. The required *d*-axis and *q*-axis negative-sequence rotor currents, with respective to the negative-sequence stator voltage reference frame [10], are

$$I_{rd-} = (U_{s-} / U_{s+}) I_{rd+} \tag{7}$$

$$I_{rq-} = -(U_{s-} / U_{s+}) I_{rq+} \tag{8}$$

where I_{rd+} and I_{rq+} stand for the *d*-axis and *q*-axis positive-sequence rotor currents, U_{s+} and U_{s-} stand for the positive- and negative-sequence stator voltage magnitudes.

Per several grid codes such as [27], the priority is on the injection of additional positive-sequence reactive current during faults. Considering the limitations in [10], I_{rq+} has the priority, thus I_{rd+} and I_{rq+} can be simplified as

$$I_{rd+} \approx 0 \quad I_{rq+} \approx -\frac{U_{s+}}{U_{s+} + U_{s-}} I_{\mathrm{RSC\_max}} \tag{9}$$

Substituting (9) into (7) and (8), I_{rd-} and I_{rq-} become

$$I_{rd-} = 0 \quad I_{rq-} = \frac{U_{s-}}{U_{s+} + U_{s-}} I_{\mathrm{RSC\_max}} \tag{10}$$

Substituting (10) into the negative-sequence model of the DFIG in [25], the negative-sequence stator current can be obtained as

$$I_{sd-} = 0 \quad I_{sq-} = \frac{U_{s-}}{\omega_1 L_s} - \frac{L_m}{L_s} \frac{U_{s-}}{U_{s+} + U_{s-}} I_{\mathrm{RSC\_max}} \tag{11}$$

Transforming (11) into the negative synchronous reference frame and using conjugate complex according to [10], the negative-sequence current phasor can be obtained as

$$\dot{I}_{s-} = (I_{sd-} - jI_{sq-}) e^{j\angle \dot{U}_{s-}} = -j\left(\frac{1}{\omega_1 L_s} - \frac{L_m}{L_s} \frac{I_{\mathrm{RSC\_max}}}{U_{s+} + U_{s-}}\right) \dot{U}_{s-} \tag{12}$$

Substituting the practical parameters of Table I into (12), the negative-sequence current phasor under a set of given voltage unbalance (U_{s+}=U_{s-}=0.187 pu) can be calculated as

$$\dot{I}_{s-} = \frac{\dot{U}_{s-}}{0.372 \angle -90^\circ} \tag{13}$$

The phasor diagram of the negative-sequence voltage and current phasors are shown in Fig. 8. It shows that, when the PNSC-Tem is employed, DFIG-based WTG contributes negative-sequence capacitive current that is 90° ahead of the negative-sequence voltage phasor. The phase relationship between $\dot{I}_{LQ}$ and $\dot{I}_{RQ}$ discussed in Section II may be the opposite of the predefined relationship in 87LQ. This is further articulated in Section IV.

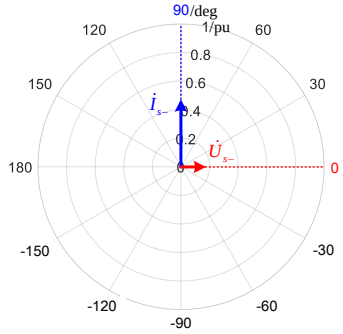

Figure 8. The phasor diagram of the negative-sequence voltage and current of a DFIG under the PNSC-Tem.

C. Negative-sequence Phasor Characteristics of DFIG-based WTG under PNSC-I12R

In recent grid codes [28] and [29], WPs are required to provide reactive current in the negative sequence system as well. The relationship with phasors is expressed as follows

$$\dot{I}_{WTG-} = -jK_{V-}\dot{U}_{s-} \tag{14}$$

where K_{V-} is the coefficient that is specified between 2 and 6.

The coordinated control implementation in [10] referred to as PNSC-I12R makes use of the maximum capacity of converters to comply with the requirements on additional reactive currents in the positive and negative sequence systems. By substituting the practical parameters of Table I into (14), and setting K_{V-} to 2, the current is given by

$$\dot{I}_{WTG-} = \frac{\dot{U}_{s-}}{0.5 \angle 90^\circ} \tag{15}$$

The phasor diagram is shown in Fig. 9. When the PNSC-I12R is employed, DFIG-based WTG contributes inductive negative-sequence current just like an inductance. According to the analysis in Section II.A, this should enable the proper functioning of 87LQ.

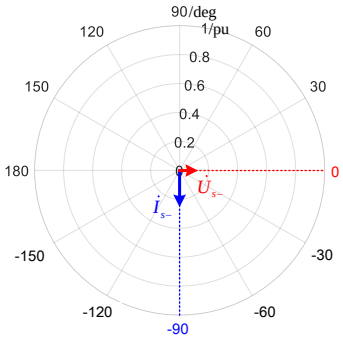

Figure 9. The phasor diagram of negative-sequence voltage and current of DFIG under PNSC-I12R.

IV. Dynamic Performance

To evaluate the dynamic performance of 87LQ under different FRT solutions, detailed time domain models of 87LQ and WP are used and transient trajectories are recorded.

A. Test System

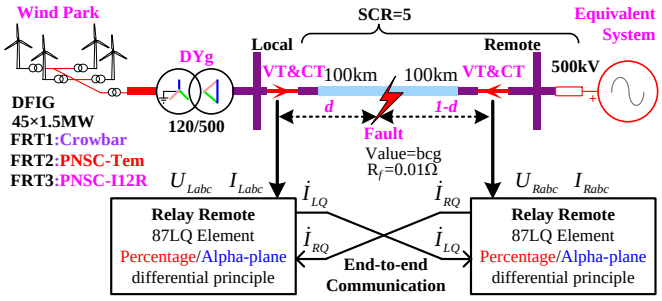

Figure 10. Single-line diagram of the 500kV 60Hz 2-bus system.

The dynamic performance of 87LQ is tested using a 500 kV, 60 Hz, 2-bus system shown in Fig. 10. A WP, consisting of 45×1.5 MW DFIG-based WTGs, is connected to the local bus through a transformer. All DFIG-based WTGs in the WP initially operate at the rated active power. The short circuit ratio (SCR) seen from the local bus is 5. A two phase to ground (BCG) short circuit is applied at the middle of the transmission line (d=0.5). Two protection relays are connected to the local and remote buses. In the model of 87LQ, the full cycle Fourier algorithm and symmetrical component method are adopted to extract negative-sequence current phasor from the three-phase instantaneous current. The basic settings of the 87LQ in both percentage and alpha-plane principles have been explained in Section II. The full details of the WP models are provided in [17] and [18]. The transient simulation results are obtained by using Simulink and Runge-Kutta fourth-order solver with a fixed time-step of 50us.

B. Impact of FRT Solutions on 87LQ Operating on Percentage Differential Principle

The dynamic performance of 87LQ operating on percentage differential principle has been described with the trajectories of I_{OP} and I_{RT} in Fig. 4 in Section II. Fig. 11, Fig. 12, and Fig. 13 show the dynamic performance of 87LQ under crowbar protection, PNSC-Tem, and PNSC-I12R.

As shown in Fig. 11, when the crowbar circuit is triggered, the trajectory quickly moves from the origin into the operating zone and a trip signal is issued. The trajectory is very close to (but not strictly on) the red dashed line which has a slope of unity representing an ideal system with conventional SGs. This indicates that, considering the impedance of transformers and lines, the angle difference between $\dot{I}_{LQ}$ and $\dot{I}_{RQ}$ is quite small (8° in this case). This is in line with the analysis in Section III.A, i.e., the WP mainly contributes inductive current in the negative-sequence system. Therefore, the crowbar protection is not expected to affect the sensitivity of 87LQ.

The trajectory in Fig. 12 is obtained under the PNSC-Tem strategy, which moves into the operating zone but quickly falls in the restraining zone. The trajectory stays in the operating zone for only 1.03 ms. Hence, 87LQ is very likely to mis operate and identify the internal BCG short circuit as an external fault since the anti-disturbance component controls the final trip signal. As discussed in Section II.A and III.B, the capacitive nature of the negative-sequence current of the WP causes this maloperation. Once steady state is reached after the fault inception, the angle difference between $\dot{I}_{LQ}$ and $\dot{I}_{RQ}$ is very close to 180°. Thus, the PNSC-Tem would significantly reduce the sensitivity of 87LQ and even cause maloperation.

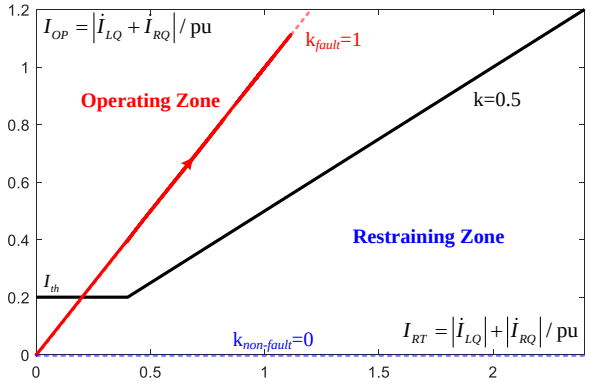

Figure 11. Dynamic performance of 87LQ operating on percentage differential principle when the crowbar protection is triggered.

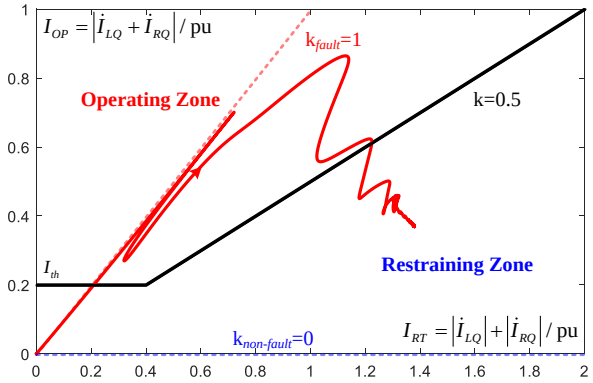

Figure 12. Dynamic performance of 87LQ operating on percentage differential principle when DFIG-based WTGs are controlled by PNSC-Tem.

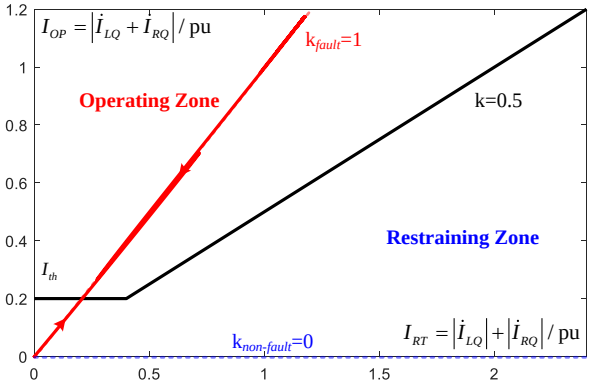

Figure 13. Dynamic performance of 87LQ operating on percentage differential principle when DFIG-based WTGs are controlled by PNSC-I12R.

The trajectory of Fig. 13 is observed under the PNSC-I12R strategy. It moves into the operating zone quickly. According to the analysis in Section II.A and III.C, the WP provides pure inductive current into the negative-sequence system just like a SG, and $\dot{I}_{LQ}$ and $\dot{I}_{RQ}$ are expected to be in phase ideally.

C. *Impact of FRT Solutions on 87LQ Operating on Alpha-plane Differential Principle*

The dynamic performance of 87LQ operating on alpha-plane principle is described with the current ratio ($\dot{I}_{RQ}$ /$\dot{I}_{LQ}$) as shown in Fig. 5 in Section II. Fig. 14, Fig. 15, and Fig. 16, respectively show the recorded dynamic performance under crowbar protection, PNSC-Tem, and PNSC-I12R.

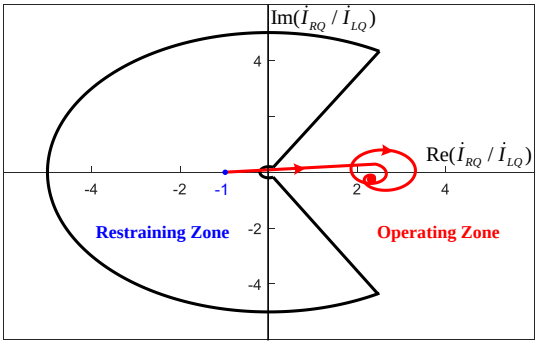

Figure 14. Dynamic performance of 87LQ operating on alpha-plane differential principle when the crowbar protection is triggered.

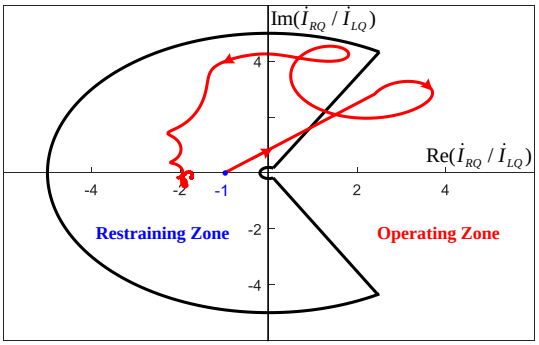

Figure 15. Dynamic performance of 87LQ operating on alpha-plane differential principle when DFIG-based WTGs are controlled by PNSC-Tem.

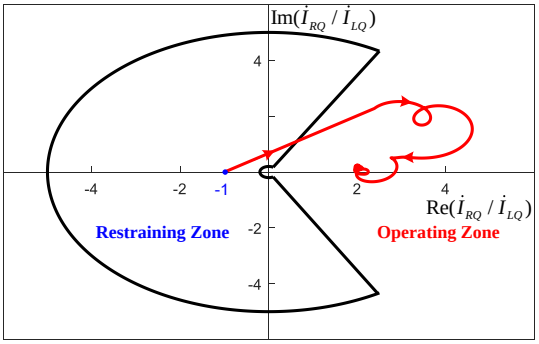

Figure 16. Dynamic performance of 87LQ operating on alpha-plane differential principle when DFIG-based WTGs are controlled by PNSC-I12R.

As shown in Fig. 14, when the crowbar circuit is triggered, the trajectory quickly moves from -1 to the positive real axis. Although oscillations are present during the first few cycles, their magnitude is low. Thus, 87LQ quickly issues a trip signal.

As shown in Fig. 15, when the PNSC-Tem is employed, the trajectory moves from -1 into the operating zone but quickly comes back to the restraining zone. During the transient, the trajectory only stays in the operating zone for 1.03 ms. The trajectory eventually lands in the negative real axis as a result of the negative-sequence capacitive current discussed in Section II.A and III.B.

As shown in Fig. 16, when the PNSC-I12R is employed, the trajectory quickly moves into the operating zone and 87LQ issues the tripping signal correctly. However, when compared to Fig. 14, the trajectory in Fig. 16 has more oscillations in the first few cycles. This transient is related to the dynamics of the current control and phase-lock loop (PLL).

V. Maloperation and Impact Factors

This section further studies the impact of fault location (represented by *d*) and the strength of the power grid (represented by SCR) on the maloperation detected in Section IV. The results help understand in what scenario the 87LQ maloperation is more likely to happen.

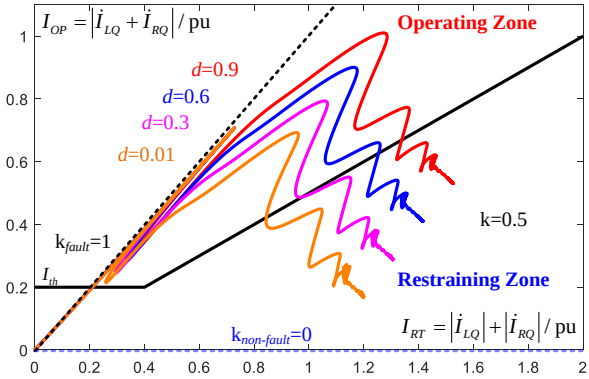

Figure 17. Dynamic performances of 87LQ operating on percentage differential principle for different fault locations. (SCR=5 and DFIG-based WTGs are controlled by PNSC-Tem)

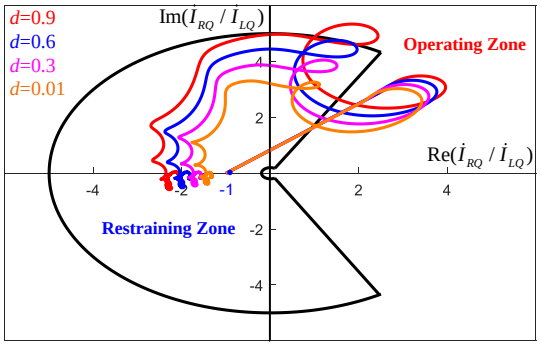

Figure 18. Dynamic performance of 87LQ operating on alpha-plane differential principle for different fault locations. (SCR=5 and DFIG-based WTGs are controlled by PNSC-Tem)

The dynamic performances of 87LQ elements for different fault locations are compared in Fig. 17 and Fig. 18. The results show that all trajectories land in the restraining zone and both types of 87LQ elements mis operate as long as the BCG short circuit is on the protected transmission line.

After changing the SCR of the test system from 5 to 10, two types of 87LQ elements are examined in a strong system scenario, i.e., capable of supplying larger amounts of short circuit currents. The dynamic performances for different fault locations are compared in Fig. 19 and Fig. 20. The results show that the trajectories are more likely to land in the restraining zone when the short circuit is close to the WP (local bus). Moreover, the 87LQ element operating on percentage principle can correctly trip the internal short circuit, while the 87LQ element operating on alpha-plane principle can only correctly operate when d>0.3.

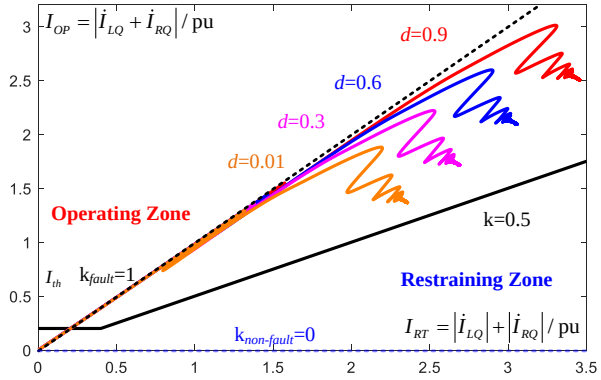

Figure 19. Dynamic performances of 87LQ operating on percentage differential principle for different fault locations. (SCR=10 and DFIG-based WTGs are controlled by PNSC-Tem)

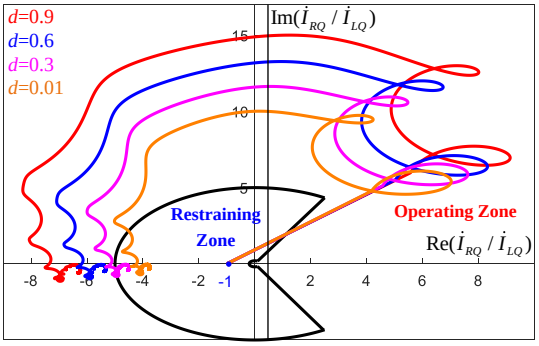

Figure 20. Dynamic performance of 87LQ operating on alpha-plane differential principle for different fault locations. (SCR=10 and DFIG-based WTGs are controlled by PNSC-Tem)

The above results indicate the maloperation is more likely to happen for weaker systems and BCG short circuits close to WP. Moreover, 87LQ element operating on alpha-plane principle is more likely to mis operate compared to the element based on the percentage principle. These observations are related to the magnitudes of $\dot{I}_{RQ}$ and $\dot{I}_{LQ}$. The magnitude of $\dot{I}_{LQ}$ is limited by the WP (0.2~0.4 pu in this case), while the magnitude of $\dot{I}_{RQ}$ can be quite significant in stronger systems. As a result, although $\dot{I}_{RQ}$ and $\dot{I}_{LQ}$ are 180° out of phase, the trajectory can easily land in the operating zone as the magnitude ratio between $\dot{I}_{RQ}$ and $\dot{I}_{LQ}$ exceeds the threshold (R for the alpha-plane differential principle, k for the percentage differential principle).

VI. Conclusions

In this paper, the dynamic performance of two different 87LQ schemes protecting a transmission line connected to a DFIG-based WP are studied under unsymmetrical fault scenarios. It is discovered that, when the WP employs a control strategy to eliminate the double grid frequency oscillations in Tem, 87LQ is likely to misinterpret internal short circuits as external faults and mis operate. The cause of this maloperation is explained by examining the relationship between the negative-sequence voltages and currents of DFIG-based WPs under three different FRT strategies. The main conclusions are summarized as follows,

(1) In power systems with conventional SGs, 87LQ has excellent sensitivity when protecting a transmission line against unsymmetrical faults, as the angle difference between $\dot{I}_{LQ}$ and $\dot{I}_{RQ}$ is close to 0° under internal faults and 180° under external faults. This kind of phase relationship is achieved since the negative-sequence system is highly inductive in SG dominant systems.

(2) Unlike SGs, the representation of DFIG-based WPs changes with different FRT solutions in the negative sequence system. When the crowbar protection is triggered, the negative-sequence current lags the negative-sequence voltage by an angle of about 75°, thus the DFIG can be represented with a fixed inductive reactance in series with a resistance in the negative-sequence network. When the PNSC-Tem is employed to eliminate the double grid frequency oscillations in electromagnetic torque, the negative-sequence current leads the negative-sequence voltage by 90°, thus the DFIG provides capacitive current into the negative-sequence network. When the PNSC-I12R is employed to comply with some recent grid codes on the requirement of additional negative-sequence reactive current, the negative-sequence current lags the negative-sequence voltage by 90°, thus the DFIG behaves like a SG.

(3) The existing percentage and alpha-plane differential principles used in 87LQ can correctly detect unsymmetrical short circuits occurring on the protected transmission line connected to a DFIG-based WP when crowbar protection or PNSC-I12R is employed.

(4) The sensitivity of 87LQ is significantly affected when a DFIG-based WP employs PNSC-Tem. During an internal unsymmetrical fault, the dynamic trajectories in percentage and alpha-plane diagrams eventually land in the restraining zones and interrupt the trip. This is caused by the negative-sequence capacitive current contributed by the WP. The phase relationship between $\dot{I}_{LQ}$ and $\dot{I}_{RQ}$ is changed in this scenario.

(5) Owing to the magnitude relationship between $\dot{I}_{LQ}$ and $\dot{I}_{RQ}$, the maloperation related to PNSC-Tem is more likely to happen for weaker systems and faults close to the WP.

REFERENCES

[1] "IEEE Standard Electrical Power System Device Function Numbers, Acronyms, and Contact Designations," in *IEEE Std C37.2-2008 (Revision of IEEE Std C37.2-1996)*, vol., no., pp.1-48, 3 Oct. 2008.

[2] B. Kasztenny, N. Fischer and H. J. Altuve, "Negative-sequence differential protection - principles, sensitivity, and security," *2015 68th Annual Conference for Protective Relay Engineers*, College Station, TX, USA, 2015, pp. 364-378.

[3] "IEEE Guide for Application of Digital Line Current Differential Relays Using Digital Communication," in *IEEE Std C37.243-2015*, vol., no., pp.1-72, 7 Aug. 2015.

[4] J. Roberts, D. Tziouvaras, G. Benmouyal, and H. Altuve, "The Effect of Multiprinciple Line Protection on Dependability and Security," in *Proc. 55th Annual Georgia Tech Protective Relaying Conference*, Atlanta, GA, May 2001.

[5] H. Miller, J. Burger, N. Fischer and B. Kasztenny, "Modern line current differential protection solutions," *2010 63rd Annual Conference for Protective Relay Engineers*, College Station, TX, USA, 2010, pp. 1-25.

[6] SEL-411L Relay – Protection and Automation System, Instruction Manual, Schweitzer Engineering Laboratories, 20170403.

[7] G. Benmouyal, "Securing Sequence-current Differential Elements," in *Proc. 31st Annual Western Protective Relay Conference*, Spokane, WA, October 2004.

[8] G. Benmouyal, "The Trajectories of Line Current Differential Faults in the Alpha Plane," in *Proc. 32nd Annual Western Protective Relay Conference*, Spokane, WA, October 2005.

[9] J. Luo, H. Zhao, X. Lu, S. Gao, Q. Ma and V. Terzija, "A Review of Low Voltage Ride Through in DFIG under Unbalanced Grid Faults," *2019 IEEE PES GTD Grand International Conference and Exposition Asia (GTD Asia)*, Bangkok, Thailand, 2019, pp. 718-723.

[10] Y. Chang, I. Kocar, J. Hu, J. Mahseredjian, K. W. Chan and U. Karaagac, "Coordinated Control of DFIG Converters to Comply with Reactive Current Requirements in Emerging Grid Codes," in *Journal of Modern Power Systems and Clean Energy*. vol. 10, no. 2, pp. 502-514, March 2022.

[11] A. Haddadi, M. Zhao, I. Kocar, U. Karaagac, K. W. Chan and E. Farantatos, "Impact of Inverter-Based Resources on Negative Sequence Quantities-Based Protection Elements," in *IEEE Transactions on Power Delivery*, vol. 36, no. 1, pp. 289-298, Feb. 2021.

[12] Y. Xue, B. Kasztenny, D. Taylor and Y. Xia, "Series compensation, power swings, and inverter-based sources and their impact on line current differential protection," *2013 66th Annual Conference for Protective Relay Engineers*, College Station, TX, USA, 2013, pp. 80-91.

[13] B. Han, H. Li, G. Wang, D. Zeng and Y. Liang, "A Virtual Multi-Terminal Current Differential Protection Scheme for Distribution Networks With Inverter-Interfaced Distributed Generators," in *IEEE Transactions on Smart Grid*, vol. 9, no. 5, pp. 5418-5431, Sept. 2018.

[14] S. Fei and T. C. Fen, "Application of differential protection to offshore wind farm for earth fault detection with substantially unbalanced charging current", *The Journal of Engineering*, vol. 2018, no. 15, pp. 836-840, 2018.

[15] A. Haddadi, E. Farantatos, I. Kocar and U. Karaagac, "Impact of Inverter Based Resources on System Protection," in *Energies*, vol. 2021, no. 14, pp. 1-22, Feb. 2021.

[16] "Impact of Inverter-Based Resources on Protection Schemes Based on Negative Sequence Components". Palo Alto, CA: EPRI, 2019.

[17] "Impact of Renewables on System Protection: Wind/PV Short-Circuit Phasor Model Library and Guidelines for System Protection Studies". Palo Alto, CA: EPRI, 2016.

[18] A. Haddadi, I. Kocar, T. Kauffmann, U. Karaagac, E. Farantatos and J. Mahseredjian, "Field validation of generic wind park models using fault records," in *Journal of Modern Power Systems and Clean Energy*, vol. 7, no. 4, pp. 826-836, July 2019.

[19] Kevin W. Jones, Pouyan Pourbeik, Gary Kobet et al, "Impact of Inverter Based Generation on Bulk Power System Dynamics and Short-Circuit Performance," Task Force on Short-Circuit and System Performance Impact of Inverter Based Generation, Tech. Rep. PES-TR68, July. 2018.

[20] A. Haddadi, M. Zhao, I. Kocar, U. Karaagac, K. W. Chan and E. Farantatos, "Impact of Inverter-Based Resources on Negative Sequence Quantities-Based Protection Elements," in *IEEE Transactions on Power Delivery*, vol. 36, no. 1, pp. 289-298, Feb. 2021.

[21] Y. Chang, J. Hu, G. Song, X. Kong and Y. Yuan, "Impact of DFIG-based wind turbine's fault current on distance relay during symmetrical faults," in *IET Renewable Power Generation*, vol. 14, no. 66, pp. 3097-3102, Dec. 2020.

[22] SEL-411L-2 – Line Current Differential Protection Automation and Control System with Sampled Values or TiDL Technology Data Sheet, Schweitzer Engineering Laboratories, 20210723.

[23] S. Engelhardt, J. Kretschmann, J. Fortmann, F. Shewarega, I. Erlich and T. Neumann, "Capability and limitations of DFIG based wind turbines concerning negative sequence control," *2013 IEEE Power & Energy Society General Meeting*, Vancouver, BC, Canada, 2013, pp. 1-5.

[24] Y. Chang, J. Hu and X. Yuan, "Mechanism Analysis of DFIG-Based Wind Turbine's Fault Current During LVRT With Equivalent Inductances," in *IEEE Journal of Emerging and Selected Topics in Power Electronics*, vol. 8, no. 2, pp. 1515-1527, June 2020.

[25] L. Xu, "Enhanced Control and Operation of DFIG-Based Wind Farms During Network Unbalance," in *IEEE Transactions on Energy Conversion*, vol. 23, no. 4, pp. 1073-1081, Dec. 2008.

[26] J. Hu, H. Xu and Y. He, "Coordinated Control of DFIG's RSC and GSC Under Generalized Unbalanced and Distorted Grid Voltage Conditions," in *IEEE Transactions on Industrial Electronics*, vol. 60, no. 7, pp. 2808-2819, July 2013.

[27] E. ON. Netz. GmbH, "Grid Code - High and Extra High Voltage", Bayreuth, Germany, Apr. 2006.

[28] VDE, "VDE-AR-N 4120: Technical requirements for the connection and operation of customer installations to the high-voltage network (TCC high-voltage)", 2015.

[29] GB/T 19963.1-2021, "Technical specification for connecting wind farm to power system—Part 1: On shore wind power", Mar. 2021.